ISSN 1392 - 1207. MECHANIKA. 2010. Nr.4(84)

Numerical and experimental investigation on ultimate strength of cracked cylindrical shells subjected to combined loading

M. Shariati*, M. Sedighi, J. Saemi***, H.R. Eipakchi****, H.R. Allahbakhsh*****
*Shahroud University of Technology, Shahroud, Iran, E-mail: hamoon47@yahoo.com
***Shahroud University of Technology, Shahroud, Iran, E-mail: msedighi47@gmail.com
****Shahroud University of Technology, Shahroud, Iran, E-mail: jafarsemi@gmail.com
****Shahroud University of Technology, Shahroud, Iran, E-mail: hamidre2000@gmail.com
*****Shahroud University of Technology, Shahroud, Iran, E-mail: allahbakhshy@gmail.com

1. Introduction

Shell structures have been widely used in pipelines, aerospace and marine structures, large dams, shell roofs, liquid-retaining structures and cooling towers [1]. Buckling is one of the main failure considerations when designing these structures [2]. At first, researchers focused on the determination of the buckling load in the linear elastic zone, but experimental studies showed that the buckling capacity of thin cylindrical shells is much lower than the amount determined in the classic theories [3, 4]. Shell structures, like other types of structures, are usually susceptible to various types of defects and damages such as initiation and propagation of cracks, corrosion, chemical attack and time-dependent material degradation, which impair their structural soundness. The presence of cracks in a shell structure can play the role of geometrical imperfection and thus reduce the load carrying capacity of the shell structure [5-7]. El Naschie [8] considered the buckling problem of a cracked shell for the first time. The buckling load of these shells is shown to be half of that of the perfect cylinder. Numerical models of cracked cylindrical shells with various crack lengths and orientations are developed by employing the meshing scheme proposed by Vaziri [9] for cracked thin plates and shells. The post-buckling analysis of cracked plates and shells indicated that the buckling deformation could cause a considerable amplification of the stress intensity around the crack tip [10]. The result show that sensitivity of the buckling behavior of both plates and shells to the presence of defects highly depends on the loading condition. As an example, in general, the buckling behavior of the cylindrical shells under torsional loading is less sensitive to the presence of a crack than that of a similar axially compressed cylindrical shell [11]. Presence of a crack may significantly alter the buckling behavior of cylindrical shells by provoking local buckling as the dominant buckling mode of the cylindrical shell. The local buckling may precede the global buckling of cylindrical shells for crack longer than a critical length. This critical length depends on the crack orientation and the loading condition [12, 13]. The microstructure and mechanical properties of material make big influence on crack propagation [14]. The numerical approach seems to be the most promising method, as the analytical formulation of the aforementioned problem is formidably complicated. Even in the case of numerical analysis, the large number of interacting parameters and the complicated shell buckling behavior makes it quite difficult to ascertain generally applicable conclusions [15-17]. In this paper, linear and nonlinear analyses using the ABAQUS finite element software, were carried out in order to study the effect of the crack position ($C = L0/L = 0.25, 0.33, 0.5$) (see Fig. 1), crack orientation ($\theta = 0°, 30°, 45°, 60°, 90°$), crack length-to-cylindrical shell perimeter ($\lambda = a/2\pi r = 0.2,\ 0.3,\ 0.4$) and shell length-to-diameter ($L/D = 2.38, 3.57, 5.59$) ratios on the buckling and post-buckling behavior of cylindrical shells. Parameter a shows the crack length and parameter θ shows the orientation of the crack direction measured from the horizontal axis. The distance between the center of the crack and the lower edge of the shell is designated by $L0$. Additionally, several experimental buckling tests were performed using an INSTRON 8802 servo hydraulic machine, and the test results were compared with the results of the finite element method. A very good correlation between experiments and numerical simulations was observed.

2. Numerical analysis using the finite element method

The numerical simulations were carried out using the general finite element program ABAQUS 6.4-PR11. For applying boundary conditions on the edges of the cylindrical shells, two rigid plates were used that were attached to the ends of the cylinder.

2.1. Geometry and mechanical properties of the shells

For this study, steel cylindrical shells with three different lengths (L = 100, 150, 250 mm), and two different diameters (D = 42, 50mm) were analyzed. The cracks in various lengths and several orientations ($\theta = 0°, 30°, 45°, 60°, 90°$) were created in the specimens. Furthermore, the thickness of shells was t = 2 mm. Fig. 1 shows the geometry of the cracked cylindrical shell.

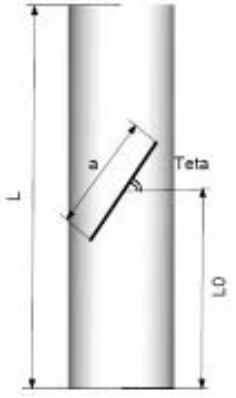

Fig. 1 Geometry of cracked cylindrical shells

Specimens were nominated as follows: $L250$-$D42$- $\theta 45°$-$\lambda 0.4$-$C0.5$. The numbers following L and D show the length and the diameter of the specimen, respectively. The parameter $C = L0/L$ ratio show the crack position.

The cylindrical shells used for this study were made of a mild steel alloy. The mechanical properties of this steel alloy were determined according to ASTM E8 standard [18], using the INSTRON 8802 servo hydraulic machine. The stress-strain curves, stress-plastic strain curve and respective values are shown in Fig. 2. Based on the linear portion of stress-strain curve, the value of elasticity module was computed as $E = 195$ GPa and the value of yield stress was obtained $\sigma_y = 340$ MPa. Furthermore, the value of Poisson's ratio was assumed to be $v = 0.33$.

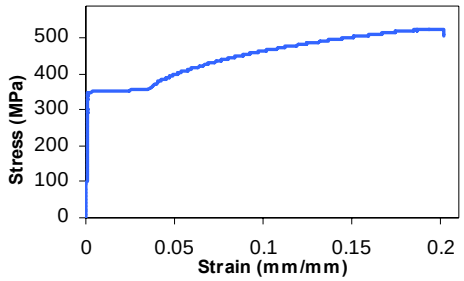

Fig. 2 Stress-strain diagram of steel alloy

2.2. Element formulation of the specimens

For this analysis, the nonlinear element S8R5, which is an eight-node element with six degrees of freedom per node, suitable for the analysis of thin shells, and the linear element S4R, which is a four-node element were used. Part of a meshed specimen is shown in Fig. 3.

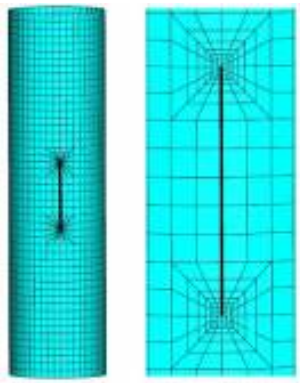

Fig. 3 Sample of FEM mesh

2.4. Analytical process

In cracked plate and shell problems modeling of the singular stress field at the crack tip two different approaches can be applied [19].

Primary modes have smaller eigenvalues and buckling usually occurs in these mode shapes. For eigenvalues analysis the ''Buckle'' step was used in software. It is noteworthy that due to the presence of contact constraints between rigid plates and the shell, the Lanczos solver method cannot be used for these specimens [20]. In Fig. 4, two primary mode shapes are shown for the specimen $L150$-$D42$- $\theta 90°$.

After completion of the Buckle analysis, a nonlinear analysis was performed to plot the load-displacement

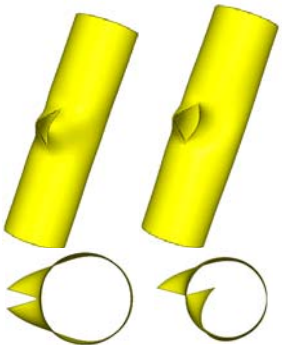

a b

Fig. 4 Buckling mode shape for specimen $L150$-$D42$-$\theta 90°$: a - first mode, b - second mode

curve. This step is called ''Static Riks'' and uses the arc length method for post-buckling analysis. In this analysis, nonlinearity of both material properties and geometry is taken into consideration.

2.5. Reference cylindrical shell

For plotting of the curves, it is preferable to use dimensionless data. In this study, for making the buckling load dimensionless, we used buckling of a reference cylindrical shell, which is defined as follows

$$F_{ref} = \pi D t \quad \sigma_y$$

where F_{ref} is the reference load, which is in fact the load required for the cylindrical shell to yield; D is the diameter; t is the thickness of the shells; σ_y is yield stress of the material used in the making of shells. Therefore, the reference load of the specimens is calculated in this way

$$F_{ref} = \pi \times 42 \text{ mm} \times 2 \text{ mm} \times 340 \text{ N/mm}^2 = 89.964 \text{ kN}$$

Also, the amount of compressive deformation of the shells was made dimensionless using the length of the shells.

3. Numerical analysis results

In this section, the results of the buckling analysis in cylindrical shells, with a crack in different length, orientation and positions were presented. For this purpose, the crack with three length ($\lambda = 0.2$, 0.3, 0.4) and various orientation ($\theta = 0°$, 30°, 45°, 60°, 90°) was created on the shells. As mentioned previously, the boundary conditions are symmetric with reference to the mid-height of shells. Therefore, when the crack is located along half of the shell length, due to the presence of symmetry, it would reflect the influence of the crack's location along the entire length of the shells. The designation and analysis details of each model are summarized in Table 1. Evidently, the results of this analysis can be generalized to the shells with similar L/D and D/t and λ ratios.

The results show that a change in position of the crack, affects the buckling load. Figs. 5 and 6 show the load-end shortening curves, isometric and top views of the shells and von Mises stress contours for two specimens with ratios $L/D = 21$ and $\lambda = 0.3$, with a crack of fixed size in different positions ($L0/L = 0.5$ and 0.33). According to Figs. 5 and 6, it can be seen that before the load reaches a critical value, stress is uniformly distributed in all areas of

Table 1
Summary of numerical analysis for cracked cylindrical shells

Model designation	Shell length	Crack length $a/2\pi r$	Crack location L_0/L	Crack orientation	Buckling load, kN	
					S4R element	S8R5 element
*D*42-*L*100-Perfect	100	-	-	-	111.15	109.47
*D*42-*L*100-*θ*0-*λ*0.3	100	0.3	0.5	0°	105.24	102.06
*D*42-*L*100-*θ*45-*λ*0.3	100	0.3	0.5	45°	85.90	83.79
*D*42-*L*100-*θ*90-*λ*0.4	150	0.4	0.5	90°	94.37	92.24
*D*42-*L*150-*θ*45-*λ*0.3	150	0.3	0.5	45°	81.05	78.94
*D*42-*L*150-*θ*90-*λ*0.3	150	0.3	0.5	90°	98.15	92.71
*D*42-*L*150-*θ*90-*λ*0.4	150	0.4	0.5	90°	90.39	88.95
*D*42-*L*150-*θ*60-*λ*0.4	150	0.4	0.5	60°	89.73	89.14
*D*42-*L*150-*θ*90-*λ*0.3	150	0.3	0.25	90°	95.17	92.97
*D*42-*L*150-*θ*90-*λ*0.3	150	0.3	0.33	90°	98.04	94.65
*D*42-*L*250-*θ*45-*λ*0.3	250	0.3	0.5	45°	79.32	78.82
*D*42-*L*250-*θ*90-*λ*0.3	250	0.3	0.5	90°	92.01	87.68
*D*42-*L*250-*θ*60-*λ*0.4	250	0.4	0.5	60°	85.27	85.63
*D*42-*L*250-*θ*30-*λ*0.4	250	0.4	0.5	30°	84.72	85.12
*D*50-*L*100-*θ*90-*λ*0.4	150	0.4	0.5	90°	115.79	112.09
*D*50-*L*150-*θ*45-*λ*0.3	150	0.3	0.5	45°	107.83	105.63
*D*50-*L*150-*θ*90-*λ*0.3	150	0.3	0.5	90°	114.36	112.39
*D*50-*L*150-*θ*90-*λ*0.3	150	0.3	0.33	90°	112.73	109.75
*D*50-*L*250-*θ*0-λ0.2	250	0.2	0.5	0°	111.25	110.17
*D*50-*L*250-*θ*45-λ0.3	250	0.3	0.5	45°	103.67	102.91
*D*50-*L*250-*θ*90-λ0.4	250	0.4	0.5	90°	104.35	103.07

the shell, except the regions around the crack, and it increases with increasing load. In the specimen with a crack in mid-height position, stress contours are totally symmetrical. The front region of the shell tolerates less stress because of the presence of the crack (Figs. 5, a and 6, a), and the area of these regions increases with increase in load, until the load reaches the critical value. However, in regions around the crack and in circumferential direction of the shell, stress rises briskly, so that these regions yield before the shell reaches the buckling state (Figs. 5, b and 6, b). The front region of the shell tolerates less stress because of the presence of the crack (Figs. 5, a and 6, a), and the area of these regions increases with increase in load, until the load reaches the critical value. However, in regions around the crack and in circumferential direction of the shell, stress rises briskly, so that these regions yield before the shell reaches the buckling state (Figs. 5, b and 6, b). Comparing Figs. 5 and 6, it can be deduced that with increasing *L*0/*L* ratio, stress distribution becomes more uniform before and after buckling, so that it approaches uniform stress distribution in the shell, except for the regions around the crack.

This can be the reason for the observation that buckling load increases with the increase in *L*0/*L* ratio. It can be seen that first the buckling occurs locally and then the shell experiences generalized bending. The FEM results also confirm this statement, since the obtained values for rotational displacements of the shell around an axis perpendicular to its longitudinal axis. These curves are produced from finite element analyses with linear element S4R; because these elements have the post-buckling region better than other elements, according to the comparison done in section 4 between numerical and experimental results. Result show that with changing the position of the

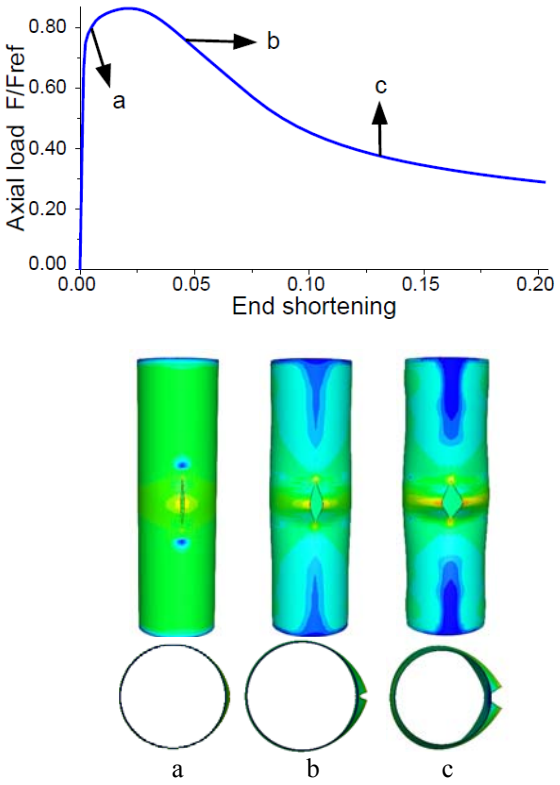

Fig. 5 Plots of load vs. end shortening, the shell deformations and the von Mises stress states at various loading stages of the specimen *D*42-*L*150- *θ*90- *λ*0.3-*C*0.5

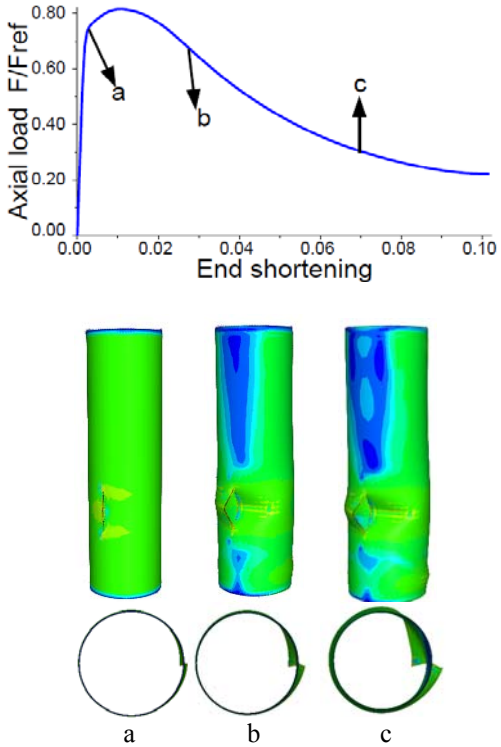

Fig. 6 Plots of load vs. end shortening, the shell deformations and the von Mises stress states at various loading stages of the specimen *D*42-*L*150- *θ*90- *λ*0.3-*C*0.5

crack from mid-height of the shell toward the *L*0/*L* = 0.33, buckling mode shapes are changed.

3.1. The effect of crack orientation on the buckling behavior of cracked cylindrical shells

In this section, the effect of crack orientation on the buckling behavior of cracked cylindrical shells under axial compression is studied by emphasizing on three crack orientations of 0°, 45° and 90°, measured from the circumferential line of the cylindrical shell. Circumferential crack $\theta = 0°$ has a small effect on the reduction of buckling load, because after the cylindrical shell is loaded, two edges of the crack place on each other and the cylinder behaves similar to perfect and non cracked shell. The circumferential crack, for three different lengths of cylindrical shell, only causes 8% reduction in the critical buckling load. Also increasing the ratio of crack length to perimeter λ from 0.2 to 0.4 has a negligible effect on buckling load reduction. The crack with the angle $\theta = 45°$ has the most effect on reducing the buckling load and at the maximum crack length ratio $\lambda = 0.4$, the critical load for a shell of length ($L = 100$ mm) reduces to 73% of the buckling load of perfect cylinder. This value for lengths $L = 150$ and 250 mm is respectively 69% and 63% of the buckling load of the cylinder with the same length and without crack.

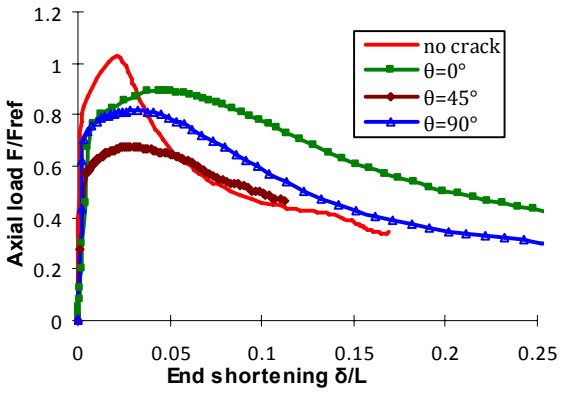

a

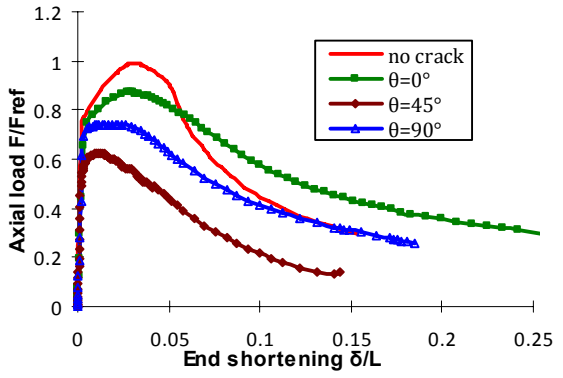

b

Fig. 7 Load-end shortening behavior of cylindrical shells with and without crack at various crack angles a - $L150$-$\lambda 0.4$, b - $L250$-$\lambda 0.4$

While loading for the longitudinal crack $\theta = 90°$, no interaction is generated between two crack edges and those edges open completely. For the same crack length, the influence of longitudinal crack on the critical buckling load is more than circumferential crack and less than oblique crack. Fig. 7 shows the numerical results of crack angle effect on the critical buckling load.

3.2. The effect of crack length on the buckling behavior of cracked cylindrical shells

The effect of crack length on buckling behavior and post buckling of cracked shell is shown in Fig. 8. This effect is more on larger length cylinders. The effect of longitudinal crack $\theta = 90°$ on buckling load reduction increases by enhancing the length of the shell. The existence of longitudinal crack with the ratio of $\lambda = 0.4$ on the cylindrical shell with the length of $L = 250$ mm reduces the shell buckling load to 76% of the buckling load of perfect cylinder. In longitudinal crack, the change in crack length and increasing λ has minor effect on the buckling load. Opposite of horizontal and oblique cracks, in longitudinal crack, no interaction exists between the two crack edges while deformation of the shell and the crack opens completely.

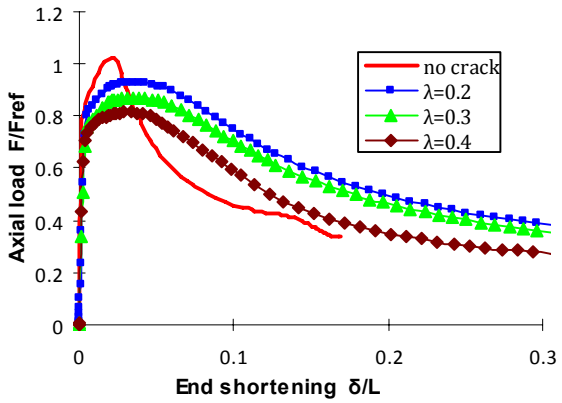

a

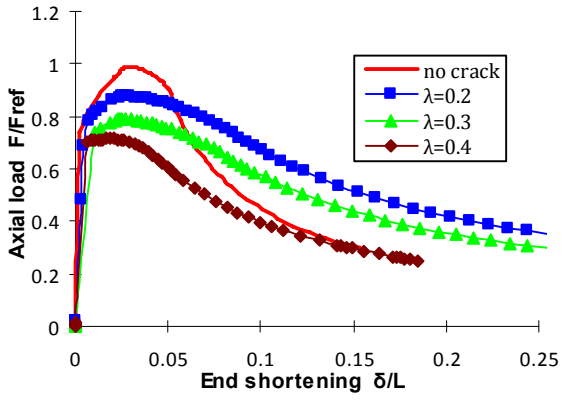

b

Fig. 8 Load-end shortening behavior of cylindrical shells with and without crack at various crack length: a – $L150 - \theta = 45°$, b – $L250 - \theta = 90°$

That is the reason for post buckling behavior of the shells with longitudinal crack $\theta = 90°$ is so similar to each other and the difference between them is only in maximum value of the buckling force.

3.3. The effect of shell length on critical buckling load

Increasing the length of the shell reduces the critical buckling load. Fig. 9 shows the effect of both shell length and crack angle on the critical buckling load. First, by increasing the crack angle from 0° to 45°, the buckling

load decreases uniformly and at θ = 45°, it has the minimum value. Then, by increasing the angle to 60°, the buckling load increases. Enhancing the crack angle from 60° to 90° has negligible effect on the buckling load and the critical bucking load remains almost constant. It is seen that by increasing the shell length, the effect of angle 45° on reducing the critical buckling load will increase. Primary modes have smaller eigenvalues and buckling usually occurs in these mode shapes. Fig. 10 shows the effect of crack length on buckling load at different crack orientation θ = 0°-90°.

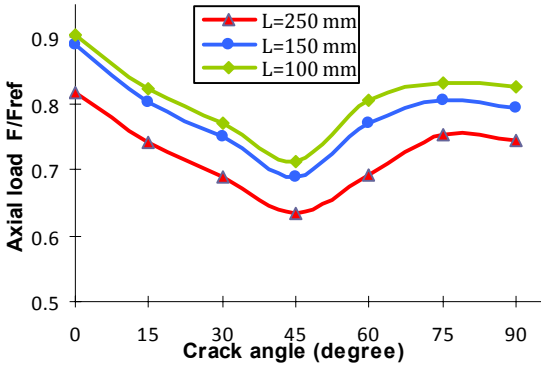

Fig. 9 Normalized buckling load of cracked shells versus crack angle and λ = 0.4

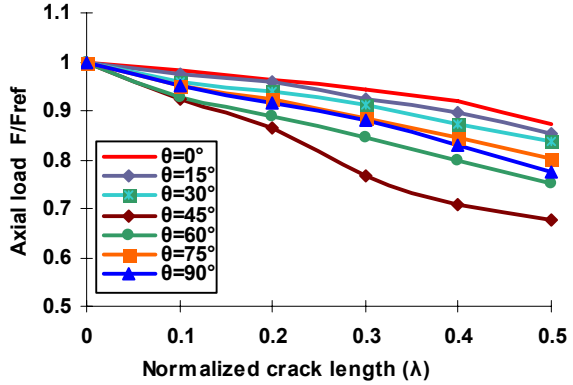

Fig. 10 Normalized buckling load of cracked shells versus crack length λ – L = 150 mm

It is seen that by increasing the crack length, the effect of angle 45° on reducing the critical buckling load will increase and increasing the crack length for circumferential crack θ = 0° has a small effect on the reduction of buckling load.

4. Confirmation of numerical results with experimental findings

In order to validate the numerical results, several tests have been performed. The crack generated empirically over the shell is in fact a very small rectangular opening whose length is the same as the crack and its width is at most 0.4 mm. For determining the maximum error produced by this assumption, the empirically generated crack with the largest opening width is considered. The numerical results show that the maximum value of error in the buckling load is 0.9% which can be clearly ignored and it also shows the accuracy in manufacturing the empirical prototypes.

Experimental tests were performed on a large number of specimens in order to confirm the numerical results. For these tests, a state-of-the-art, servo hydraulic, INSTRON 8802 machine was used. The specimens were constrained by steel sleeve fixtures inserted at both ends (Fig. 11) in the experimental test, for the simulation of combined loading, it will be shown that the fulcrum used in these tests in Fig. 14.

Fig. 11 Fixtures for experimental test

The results of experiments are compared with numerical findings in Table 2. It is evident from Table 2 that there is a little difference between experimental and numerical results. For example, the biggest discrepancy between the two sets of results is 4.74% for S8R5 nonlinear element and 3.87% for S4R linear element. It is also noteworthy that the greatest difference is seen for short specimens.

This can be attributed to the fact that the bending theory of shells is more suitable for lower t/L ratios, and this theory is used by the software for calculations the mean difference between the numerical calculations and the experimental results is 2.86% for S4R element and 2.35% for S8R5 element. It can be said that the results of analysis with nonlinear elements have lower errors the

Table 2
Comparison of the experimental and numerical results for cracked cylindrical shells

Model designation	Buckling load, kN			Error = (F_{FEM}-F_{EXP}/ F_{EXP}) x x 100	
	S4R element	S8R5 element	Experimental	S4R element	S8R5 element
*D*42-*L*100-Perfect	111.15	109.47	114.92	3.28	4.74
*D*42-*L*100-*θ*0-*λ*0.2	107.83	106.50	110.07	2.03	3.25
*D*42-*L*100-*θ*0-*λ*0.3	105.24	102.06	103.15	2.01	1.05
*D*42-*L*100-*θ*45-*λ*0.2	98.62	95.39	96.81	1.87	1.46
*D*42-*L*100-*θ*45-*λ*0.3	85.90	83.79	83.27	3.16	0.61
*D*42-*L*100-*θ*90-*λ*0.4	94.37	92.24	91.42	3.23	0.9
*D*42-*L*150-*θ*0-*λ*0.3	103.94	100.07	104.65	0.68	4.36
*D*42-*L*150-*θ*0-*λ*0.4	102.15	99.42	102.04	0.1	2.54
*D*42-*L*150-*θ*45-*λ*0.2	96.83	94.56	95.71	1.18	1.2
*D*42-*L*150-*θ*45-*λ*0.3	81.05	78.94	79.07	2.54	0.16
*D*42-*L*150-*θ*90-*λ*0.3	98.15	92.71	94.73	3.61	2.13
*D*42-*L*150-*θ*90-*λ*0.4	90.39	88.95	91.51	1.23	2.79
*D*42-*L*150-*θ*90-*λ*0.3	98.08	94.65	96.27	1.89	1.68
*D*42-*L*150-*θ*90-*λ*0.3	95.18	92.97	93.54	1.76	0.80
*D*42-*L*250-*θ*0-*λ*0.2	98.05	95.76	101.28	3.64	4.44
*D*42-*L*250-*θ*45-*λ*0.3	79.32	78.82	79.84	0.72	1.31
*D*42-*L*250-*θ*90-*λ*0.2	101.27	94.08	97.72	3.63	3.71
*D*42-*L*250-*θ*90-*λ*0.3	92.01	87.68	88.61	3.83	1.05
*D*42-*L*250-*θ*90-*λ*0.4	87.19	84.95	85.03	2.54	0.09

load–displacement curves produced by numerical and experimental analyses are shown in Figs. 12, 13 for three specimens. After comparing the curves in Fig. 12, it can be said that linear elements in comparison to nonlinear elements, have a better prediction power for the post-buckling behavior of mild steel alloy cylindrical shells with a crack. In the prebuckling phase, both elements produce similar results.

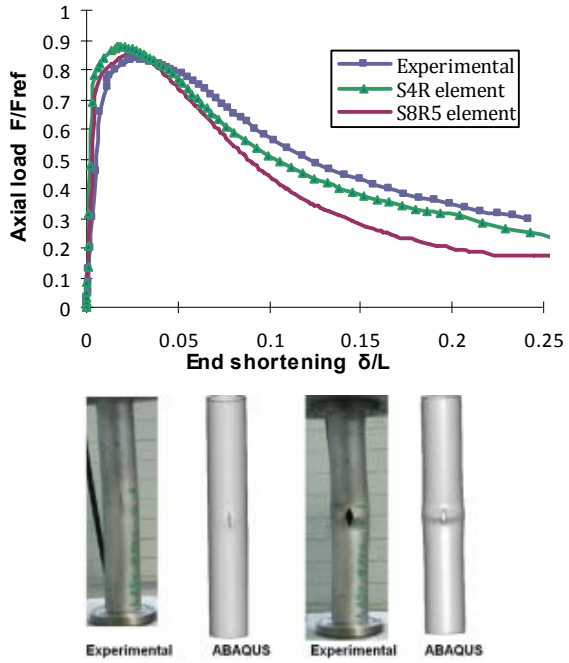

Fig. 12 Comparison of the experimental and numerical results for the specimen *D*42-*L*250- θ90- λ0.2-*C*0.5

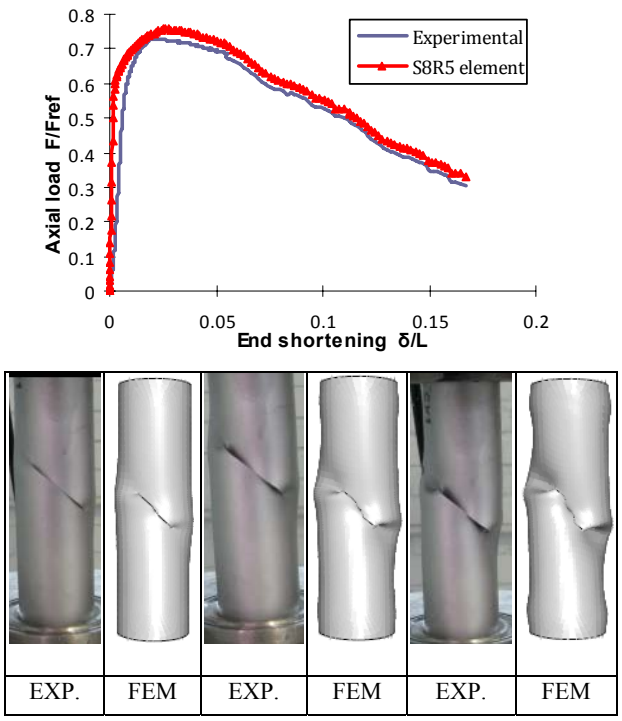

Fig. 13 Comparison of the experimental and numerical results for the specimen *D*42-*L*150- θ45- λ0.3-*C*0.5

It can be seen that the slope of load vs. end shortening curves is higher in numerical results than in experimental results before the buckling. This discrepancy is due to the presence of internal defects in the material which reduces stiffness of the specimens in the experimental method.

5. Effect of eccentric loading

In this section, the effect of eccentric loading (Fig. 14) on the buckling behavior of cracked cylindrical shells under axial compression is studied by emphasizing on three crack orientations of 0°, 45° and 90°, measured from the circumferential line of the cylindrical shell.

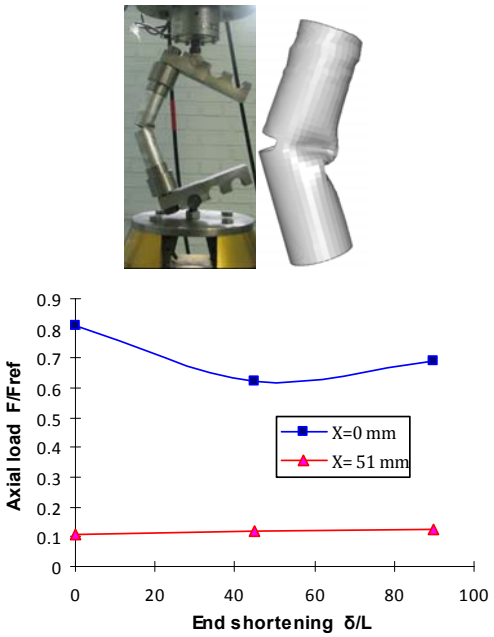

Fig. 14 Load behavior of cylindrical shells under combined loading at various crack angles

The results indicate that buckling load is more sensitivity to eccentric load and only the eccentricity (X = 51 mm) will cause the shell to buckle at 0.1 of axial compression load.

6. Concluding remarks

In this research, we studied the buckling load of steel cylindrical shells of various L/D ratios with the crack in different length and orientation using numerical and experimental methods. Also the buckling load of these cracked shells is determined with a crack in different positions. The following results were found in this study.

1. Changing the position of the crack from the mid-height of the shell toward the edges decreases the buckling load, and longer shells are more sensitive to the change in crack position.
2. Increasing the shell diameter with a fixed thickness increased the buckling load. And an increase in the L/D ratio reduces the buckling load.
3. For cracked cylindrical shells with a crack, at first the buckling occurs locally, and then the shell experiences general bending.
4. Presence of a crack may significantly alter the buckling behavior of cylindrical shells by provoking local buckling as the dominant buckling mode of the cylindrical shell.
5. The local buckling may precede the global

buckling of cylindrical shells for crack longer than a critical length. This critical length depends on the crack orientation and the loading condition.

6. Comparison of the curves shows that the numerical and experimental results are well matched. Furthermore, the curves from linear elements predict the post-buckling region better than nonlinear elements, while the nonlinear elements are a better indicator of the buckling load.

7. In longitudinal crack, no interaction exists between the two crack edges while deformation of the shell and the crack opens completely. That is why the post buckling behavior of the shells with longitudinal crack is so similar to each other and the difference between them is only in maximum value of the buckling force.

8. The results show that the buckling mode of cylindrical shell with circumference crack changes by varying the crack length. Also when the crack moves along the shell, the buckling mode of the longitudinal crack changes and buckling occurs at the second mode.

9. Figure of simultaneously effect of shell length and crack angle on the critical buckling load show, First by increasing the crack angle from 0° to 45°, the buckling load decreases uniformly and at $\theta = 90°$, it has the minimum value. Then, by increasing the angle to 60°, the buckling load increases. Enhancing the crack angle from 60° to 90° has negligible effect on the buckling load and the critical bucking load remains almost constant. It is seen that by increasing the shell length, the effect of angle 45° on reducing the critical buckling load will increase.

References

1. **Farshad, M**. Design and Analysis of Shell Structures. -Dordrecht, Kluwer, 1992.-440p.
2. **Budiansky, B, Hutchinson, JW**. Buckling of circular cylindrical shells under axial compression. -Contributions to the Theory of Aircraft Structures. -Netherlands: Delft University Press, 1972, p.239-60.
3. **Arbocz, J, Hol, JMAM.** Collapse of axially compressed cylindrical shells with random imperfections. -AIAA J, 1991, 29:2247-56.
4. **Farshad, M.** Stability of Structures. -Amsterdam: Elsevier, 1994.-438p.
5. **Hutchinson, JW, Tennyson, RC, Muggeridge, DB.** Effect of local axisymmetric imperfection on the buckling of a cylindrical shell under axial compression. -AIAA J, 1972, 9:48-52.
6. **Barut, A, Madenci, A, Britt, VO, Starnes, JH.** Buckling of a thin, tension loaded, composite plate with an inclined crack. -Eng Fract Mech, 1997, 58:233-48.
7. **Vafai, A, Estekanchi, HE.** A prologue to the buckling analysis of cracked shells. -Iranian Journal of Science and Technology, 1996, 20:137-68.
8. **El Naschie, M.S.** 'Branching solution for local buckling of a circumferentially cracked cylindrical shell. -Int J Mech Sci, 1974, 16. 689-97,.
9. **Vaziri, A, Estekanchi, H.E.** 'Buckling of cracked cylindrical thin shells under combined internal pressure and axial compression'. -Thin-Walled Struct, 44, 2006, 141-151.
10. **Riks, A., Rankin, C.C., Broan, F.A.** The buckling of a central crack in a plate under tension. -Eng Fract Mech, 1992, 26. 1023-42.
11. **Estekanchi, H.E., Vafai, A.** On the buckling of cylindrical shells with through cracks under axial load. -Thin Wall Struct, 1999, 35(4):255-74.
12. **Vaziri, A.** On the buckling of cracked composite cylindrical shells under axial compression. -Composite Structures, 2007, 80, 152-158.
13. **Vaziri, A, Nayeb-Hashemi, H, Estekanchi, HE.** Dynamic response of cracked cylindrical shells with internal pressure. -Proceedings of the ASME congress and exposition, 2002.
14. **Leonavičius, M.K., Krenevičius, A., Bacevičius, J.** Influence of structure and mechanical properties for cyclic fracture rates of cast iron. -Mechanika. -Kaunas: Technologija, 2010, Nr.2(82), p.14-20.
15. **Khamlichi, A, Bezzazi, M, Limam, A**. Buckling of elastic cylindrical shells considering the effect of localized axisymmetric imperfections. -Thin Wall Struct 2004, 42(7):1035-47.
16. **Jakušovas, A. Daunys, M.** Investigation of low cycle fatigue crack opening by finite element method. -Mechanika. -Kaunas: Technologija, 2009, Nr.3(77), p.13-17.
17. **Stupak, E.** Investigation of fracture of inhomogeneous cast iron specimens. -Mechanika. -Kaunas: Technologija, 2010, Nr.1(81), p.20-24.
18. ASTM A370-05, Standard test methods and definitions for mechanical testing of steel products.
19. **Jayaswal, K, Grosse, IR.** Finite element error estimation for crack tip singular elements. Finite Elements in Analysis and Design, 1993, 14:17-35.
20. ABAQUS 6.4 PR11 user's manual.

M. Shariati, M. Sedighi, J. Saemi, H. R. Eipakchi, H. R. Allahbakhsh

SKAITMENINIS IR EKSPERIMENTINIS PLONASIENIŲ CILINDRŲ SU PLYŠIU STIPRUMO TYRIMAS ESANT KOMBINUOTAM APKROVIMUI

R e z i u m ė

Straipsnyje aprašoma skaitmeninė ir eksperimentinė plieninių plonasienių cilindrų su plyšiu klupimo priklausomai nuo cilindro ilgio ir skersmens, plyšio pozicijos, orientacijos, jo ilgio santykio su cilindro perimetru $(\lambda = a / 2\pi r)$ ir cilindro ilgio ir skersmens santykio (L/D) analizė. Baigtinių elementų metodu ištirtas cilindrų klupimo procesas. Keletas bandinių išbandyta naudojant hidraulinę mašiną INSTRON 8802. Bandymo rezultatai gerai sutapo su skaičiavimų rezultatais.

M. Shariati, M. Sedighi, J. Saemi, H. R. Eipakchi,
H. R. Allahbakhsh

NUMERICAL AND EXPERIMENTAL INVESTIGATION ON ULTIMATE STRENGTH OF CRACKED CYLINDRICAL SHELLS SUBJECTED TO COMBINED LOADING

S u m m a r y

In this paper, experimental and numerical buckling analysis of steel cylindrical shells of various lengths and diameters with crack have been studied using the finite element method and the effect of crack position, crack orientation and the crack length-to-cylindrical shell perimeter ($\lambda = a/2\pi r$) and shell length-to-diameter (L/D) ratios on the buckling and post-buckling behavior of cylindrical shells have been investigated. For several specimens, buckling test was performed using an INSTRON 8802 servo hydraulic machine and the results of experimental tests were compared to numerical results. A very good correlation was observed between numerical simulation and experimental results.

М. Шариати, М. Седигхи, Ю. Саеми, Х.Р. Эипакцхи,
Х.Р. Аллахбакхсх

ЧИСЛЕННОЕ И ЭКСПЕРИМЕНТАЛЬНОЕ ИССЛЕДОВАНИЕ ПРОЧНОСТИ ТОНКОСТЕННЫХ ЦИЛИНДРОВ С ТРЕЩИНОЙ ПРИ КОМБИНИРОВАННОМ НАГРУЖЕНИИ

Р е з ю м е

В статье представлен числовой и экспериментальный анализ устойчивости стальных тонкостенных цилиндров с трещиной в зависимости от длины и диаметра цилиндра, расположения, ориентации трещины, соотношения ее длины с периметром цилиндра $\left(\lambda = a/2\pi r\right)$, соотношения длины и диаметра цилиндра (L/D). Методом конечного элемента описан процесс потери устойчивости. Несколько образцов испытано на гидравлической машине INSTRON 8802. Сопоставление экспериментальных результатов с результатами численного анализа показало хорошее соответствие.

Received March 25, 2010
Accepted July 02, 2010

DOI: 10.5755/j02.mech.15932